HHS Public Access

Author manuscript

Nat Chem Biol. Author manuscript; available in PMC 2018 September 05.

Published in final edited form as:

Nat Chem Biol. 2018 May ; 14(5): 458–465. doi:10.1038/s41589-018-0011-x.

Regulation of apoptosis by an intrinsically disordered region of Bcl-xL

Ariele Viacava Follis[1], **Fabien Llambi**[2], **Halime Kalkavan**[2], **Yong Yao**[3], **Aaron H. Phillips**[1], **Cheon-Gil Park**[1], **Francesca M. Marassi**[3], **Douglas R. Green**[2], and **Richard W. Kriwacki**[1,4,*]

[1]Department of Structural Biology, St Jude Children's Research Hospital, 262 Danny Thomas Place, 38105, Memphis, TN, USA

[2]Department of Immunology, St Jude Children's Research Hospital, 262 Danny Thomas Place, 38105, Memphis, TN, USA

[3]Sanford Burnham Prebys Medical Discovery Institute, 10901 North Torrey Pines Road, La Jolla, CA 92037, USA

[4]Department of Microbiology, Immunology and Biochemistry, University of Tennessee Health Sciences Center, 920 Court Avenue, Memphis, TN, 38163, USA

Abstract

Intrinsically disordered regions (IDRs) of proteins often regulate function upon posttranslational modifications (PTMs) through interactions with folded domains. An IDR linking two α-helices (α1–α2) of the anti-apoptotic protein, Bcl-xL, experiences several PTMs, which reduce anti-apoptotic activity. Here, we report that PTMs within the α1–α2 IDR promote its interaction with the folded core of Bcl-xL that inhibits the pro-apoptotic activity of two types of regulatory targets, BH3-only proteins and p53. This autoregulation utilizes an allosteric pathway where, in one direction, the IDR induces a direct displacement of p53 from Bcl-xL coupled to allosteric displacement of simultaneously bound BH3-only partners. This pathway operates in the opposite direction when the BH3-only protein PUMA binds to the BH3 binding groove of Bcl-xL, directly displacing other bound BH3-only proteins, and allosterically remodeling the distal site, displacing p53. Our findings show how an IDR enhances functional versatility through PTM-dependent, allosteric regulation of a folded protein domain.

[*]**CORRESPONDING AUTHOR INFORMATION**. R.W.K.: phone (901) 595-3290, richard.kriwacki@stjude.org.

ACCESSION CODES

Data for the solution structure of Bcl-xL S62E has been deposited to the Protein Data Bank (PDB; accession code: 6BF2) and Biological Magnetic Resonance Bank (BMRB; accession code: 27291).

AUTHOR CONTRIBUTIONS

A.V.F designed experiments, performed experiments, analyzed data and wrote the manuscript; F.L. designed and performed cell experiments; H.K. designed experiments, performed experiments, and analyzed data; Y.Y. designed experiments, performed experiments, and analyzed data; A.H.P designed experiments, performed experiments, and analyzed data; C.P. F.M.M. designed experiments and analyzed data; D.R.G. designed experiments and wrote the manuscript; and R.W.K designed experiments, analyzed data and wrote the manuscript. All authors reviewed and edited the manuscript.

Competing interests

The authors declare no competing financial interests.

INTRODUCTION

Proteins are often comprised of both structured domains and intrinsically disordered regions (IDRs)[1]. Importantly, IDRs can modulate the function of folded domains through a variety of in *cis* autoregulatory mechanisms[2]. In some cases, autoregulatory IDRs serve as "lids" that occlude binding sites within folded domains for *trans* binding partners [*e.g.*, the N-terminal lid of Mdm2 that inhibits p53 binding[3]]. This type of IDR-mediated autoinhibition is often regulated by posttranslational modifications[2]. In other cases, autoregulatory IDRs can allosterically regulate the conformation and function of folded domains [*e.g.*, the C-terminal IDR of Ets-1 traps the folded DNA binding domain in a DNA binding incompetent conformation and this inhibition is relieved by multisite phosphorylation of the IDR[4]]. These two examples involve N- and C-terminal IDRs but internal regulatory IDRs have also been characterized[2]. Examples are the autoregulatory IDRs in the anti-apoptotic proteins, Bcl-xL and Bcl-2, which sequester their pro-apoptotic Bcl-2 protein family counterparts to inhibit apoptosis[5,6]. Bcl-xL and Bcl-2 utilize dual mechanisms to regulate apoptosis. First, a hydrophobic groove in Bcl-xL and Bcl-2 binds the α-helical BH3 domain of pro-apoptotic regulators, inhibiting apoptosis[7]. Second, a site distal to the hydrophobic groove in Bcl-xL binds cytosolic p53, inhibiting p53-dependent activation of BAX and apoptosis[8]. Uniquely, the BH3-only protein, PUMA, triggers apoptosis through dual mechanisms by, i) binding to the hydrophobic groove of Bcl-xL and displacing pro-apoptotic BH3-only proteins and ii) allosterically remodeling the distal binding site to release p53[9].

Posttranslational modifications within the internal IDRs, positioned between α-helices 1 and 2 (termed the "α1–α2 IDR"), modulate the anti-apoptotic function of Bcl-xL and Bcl-2[10–29] (Fig. 1a, b). One type of posttranslational modification is cleavage of the α1–α2 IDR in Bcl-xL and Bcl-2 by pro-inflammatory Caspase 1[11] or by executioner Caspase 3 during late apoptosis[13,14], which both enhance apoptosis. Another involves phosphorylation of residues within the α1–α2 IDR, which is also associated with elevated cell death. Signaling by the kinases JNK[17,18] and Cdk1[20,26,28,30], among others, has been implicated in these IDR-mediated autoregulatory mechanisms, wherein phosphorylation of the α1–α2 IDR in Bcl-xL is thought to initiate apoptosis in response to activation of the mitotic spindle checkpoint[20,23,25,26]. Additionally, phosphorylation within the α1–α2 IDR in Bcl-xL may modulate coordinated inhibition of apoptosis and autophagy[29] through sequestration of the BH3-like region of Beclin1[31]. The principal regulatory phosphorylation site within the α1–α2 IDR of Bcl-xL is serine 62 (S62)[23]. Another modification is deamidation of asparagines 52 and 66 (N52 and N66), which converts the dipeptide sequence Asn-Gly into Asp-Gly as a consequence of intracellular acidification[21]. Despite abundant data on the autoregulatory role of the α1–α2 IDR, the mechanism through which posttranslational modifications within the IDR modulate the anti-apoptotic function of Bcl-xL is unknown. Here, we used nuclear magnetic resonance (NMR) spectroscopy and several *in vitro* and cellular assays to reveal how phosphorylation of S62 or deamidation of N52 and N66 within the α1–α2 IDR, i) directly inhibit p53 binding at a proximal site and ii) allosterically inhibit binding of pro-apoptotic BH3 domains to another, distal site within the folded core of Bcl-xL. This regulatory cascade reverses the allosteric mechanism utilized by PUMA to trigger p53 release from Bcl-xL. The dual regulatory role of the α1–α2 IDR, to release both p53 and

pro-apoptotic BH3-only proteins from Bcl-xL, extends the mechanistic repertoire available to IDRs to increase the functional versatility of covalently linked, folded protein domains. This versatility enables diverse signaling inputs to tune the anti-apoptotic activity of Bcl-xL and, likely, Bcl-2 to modulate cellular apoptotic responses.

RESULTS

IDR modification lowers Bcl-xL's affinity for BH3 domains

To understand the mechanistic basis for observations that the anti-apoptotic function of Bcl-xL is modulated by posttranslational modifications within its α1–α2 IDR, we first tested whether phosphorylation of S62 or deamidation of N52 and N66 influenced the affinity of Bcl-xL for its pro-apoptotic BH3 partners. We used isothermal titration calorimetry (ITC) to determine binding affinities of synthetic peptides spanning the BH3 domains of the pro-apoptotic proteins BID and BIM for wild type Bcl-xL, a Bcl-xL S62E phosphomimetic mutant with reduced anti-apoptotic function in cells[28,29], and Bcl-xL deamidated *in vitro* at N52 and N66[32] (Fig. 1c–e; Supplementary Table 1). These constructs were truncated at residue 209 and therefore lacked the C-terminal membrane insertion domain of Bcl-xL, as used in numerous past structural studies of Bcl-xL[33–35]. This C-terminal truncated form of Bcl-xL was recently shown to structurally mimic the mitochondrial membrane-anchored form of Bcl-xL[36]. Wild type Bcl-xL bound tightly to BID and BIM BH3 peptides with dissociation constants (K_D) of 13 and 17 nM, respectively, in agreement with previous reports[8,37]. In contrast, both Bcl-xL S62E and deamidated Bcl-xL exhibited reduced affinities for BID and BIM BH3 peptides, with K_D values ranging between 61 and 340 nM. These results suggested that these modifications of the α1–α2 IDR down-regulate the anti-apoptotic function of Bcl-xL by reducing its affinity for pro-apoptotic BH3 domains.

The IDR of Bcl-xL binds to α2–α3 of its folded core

The evidence that post translational modifications altered binding to pro-apoptotic BH3 partners suggested that the α1–α2 IDR may influence the conformation of the folded, α-helical core of Bcl-xL, which displays the hydrophobic BH3 domain binding groove. Analysis using two-dimensional (2D) NMR spectroscopy revealed marked differences in the chemical shift values for residues within α2 and α3 of Bcl-xL constructs containing and lacking the unmodified α1–α2 IDR (the latter termed Bcl-xL ΔIDR; Fig. 2a, b; Supplementary Fig. 1a). Examination of published structures of Bcl-xL and Bcl-xL ΔIDR[8,9,33,38] showed that these chemical shift differences correspond to subtle repositioning of the α2–α3 segment, with α3 extending further from α4–α5 in the ΔIDR construct (Supplementary Fig. 1b). Similar chemical shift differences *versus* the 2D ^{1}H-^{15}N-TROSY spectrum of wild type Bcl-xL were observed with two α1–α2 IDR modified forms of Bcl-xL, including with the S62E mutation or deamidation of N52 and N66 (Fig. 2c, d and Supplementary Fig. 1c; Supplementary Fig. 1d–g, respectively). These perturbations were particularly pronounced in the α2–α3 region of Bcl-xL, with more sparse perturbations in the neighboring α4 and α5. These observations suggest that the IDR may cause subtle but widespread conformational changes within the hydrophobic BH3 domain binding groove comprised of these helices (Supplementary Fig. 1b).

Next, we sought to identify the regions of the α1–α2 IDR that interacted with α2 and α3 of the Bcl-xL folded core. Using ITC, we determined that synthetic peptides spanning residues 44–72 of the Bcl-xL IDR (IDR 44–72) bound in *trans* to Bcl-xL ΔIDR and that phosphorylation of S62 or deamidation of N52 and N66 (e.g., peptides with N52D and N66D) enhanced this interaction. For example, the K_D value for the IDR 44–72 peptide with N52D and N66D was 6 μM and that with phosphorylated S62 was 36 μM *versus* 270 μM with the wild type peptide (Supplementary Fig. 2a–e). Titration experiments using NMR confirmed that these modified peptides bound the helical core of ^{15}N-labeled Bcl-xL ΔIDR, with the largest chemical shift perturbations (CSPs) observed for residues in α2, α3 and α8 (Supplementary Fig. 3a–i). Further, shorter α1–α2 IDR peptides (residues 52–66) with phosphorylated S62 (IDR 52–66 pS62) or the S62E mutation caused more localized CSPs within the α2–α3 region of Bcl-xL ΔIDR (Fig. 2e, f; Supplementary Fig. 3j–m). Interestingly, the trajectories of perturbed resonances in peptide titration NMR experiments exhibited a non-linear dependence on peptide concentration, suggesting three-state behavior possibly due to a peptide binding-induced conformational change within the helical core of Bcl-xL ΔIDR (Supplementary Fig. 4a). At low concentrations of the titrated IDR peptide, most perturbed resonances of Bcl-xL ΔIDR shifted in the direction of the corresponding resonance in the spectrum of wild type, IDR-containing Bcl-xL. This observation suggests that, in the absence of IDR posttranslational modifications, the α1–α2 IDR transiently interacts in *cis* with the folded core of Bcl-xL.

To gain further insight into the structural details of the IDR-core interaction and how posttranslational modifications modulate Bcl-xL anti-apoptotic function, we monitored CSPs in ^{1}H-^{15}N TROSY spectra of ^{15}N labeled Bcl-xL ΔIDR, initially complexed with an unlabeled BID BH3 domain peptide, upon titration of the IDR 44–72 pS62 peptide (Supplementary Fig. 4b, d). A large number of resonances exhibited large CSPs and shifted towards the same frequencies as upon titration of the same peptide into apo Bcl-xL ΔIDR (Supplementary Fig. 4e). Several resonances corresponding to residues within the BH3 binding groove exhibited large CSPs towards the frequencies observed with apo Bcl-xL. This effect was especially pronounced for the resonance of R139, which is engaged in a conserved electrostatic interaction with an aspartic acid side-chain in BH3 binding partners. Correspondingly, in a competition fluorescence anisotropy assay, a fluorescein-labeled BID BH3 (FAM-BID BH3) peptide was partially displaced from Bcl-xL ΔIDR through titration of the IDR 44–72 pS62 peptide (Supplementary Fig. 4f, g). These NMR and fluorescence anisotropy titration results suggest that the interaction of the α1–α2 IDR with the folded core destabilizes complexes of Bcl-xL with pro-apoptotic BH3 partners, providing a mechanism for down-regulation of its anti-apoptotic activity. While the affinities of these in *trans* IDR – folded core interactions are considerably lower than the tight Bcl-xL – BH3 domain interactions, covalent linkage of the IDR and folded core in full length Bcl-xL would enhance the in *cis* IDR – folded core interaction, enabling allosteric inhibition of the high affinity BH3 domain – BH3 domain binding groove interaction.

IDR phosphorylation enhances binding to the folded core

We next sought a mechanistic explanation that would correlate, i) the decreased affinity of Bcl-xL for pro-apoptotic BH3 partners due to the α1–α2 IDR S62E phosphomimetic

mutation or N52 and N66 deamidation and ii) the enhanced interaction of the α1–α2 IDR with the α2–α3 region of Bcl-xL due to functionally comparable modifications (S62 phosphorylation, or N52D and N66D mutations). We analyzed published structures of apo Bcl-xL and its various BH3 bound forms, which revealed a marked repositioning of the C-terminus of α2 and the entire α3 relative to α4–α5 and other parts of the BH3 binding groove upon BH3 binding. As noted previously[8,39], this BH3 binding-induced rearrangement involves opening of the binding groove to accommodate the α-helical BH3 domain[7,33] (Fig. 3a). Based on these observations, we hypothesized that the interaction of the α1–α2 IDR with the α2–α3 region of Bcl-xL hinders groove opening and antagonizes binding to BH3 domains.

We tested this hypothesis by determining the solution structure of a modified form of the α1–α2 IDR bound to the folded core of Bcl-xL using NMR. $\{^{1}H\}$-^{15}N heteronuclear nuclear Overhauser effect (NOE) spectra for Bcl-xL with the S62E phosphomimetic mutation showed that residues within the α1–α2 IDR exhibited reduced flexibility in comparison with wild-type Bcl-xL (Supplementary Fig. 5 a–d), which allowed characterization of α1–α2 IDR—folded core interactions. The similarity of patterns and magnitudes of CSPs induced in NMR spectra of Bcl-xL ΔIDR by in *trans* titration of IDR 52–66 peptides containing S62E mutation and phosphorylated S62 (Supplementary Fig. 3l, m) indicated that these two peptides bound in *trans* to Bcl-xL ΔIDR similarly and with very similar affinities. This observation supported that the in *cis* α1–α2 IDR—folded core interaction in Bcl-xL S62E reflected that associated with phosphorylation of S62. Three dimensional ^{1}H-^{15}N or ^{1}H-^{13}C-edited NOE correlation spectroscopy (NOESY) spectra of Bcl-xL S62E exhibited many ^{1}H-^{1}H NOE cross peaks between residues in the α1–α2 IDR and others in the folded protein core, enabling structure determination of Bcl-xL S62E in a 'α1–α2 IDR inhibited' conformation (Fig. 3b, c; Supplementary Fig. 5e, f). Some of these cross peaks were also detected, with weaker intensities, in corresponding spectra of the wild type protein (Supplementary Fig. 5f). In particular, the aromatic side-chain protons of W57 exhibited numerous cross peaks with shielded methyl resonances corresponding to aliphatic residues in the core of the protein, including L150 and L108.

In the structure of Bcl-xL S62E, the aromatic side-chain of W57 and other aliphatic residues, including I51 and L59, were buried inside a small hydrophobic groove between α3 and the C-termini of α5 and α1, buttressing one face of α3 opposite from that engaged in the BH3 binding groove. The negatively charged side-chains of D61 and, particularly, E62, were positioned beside a positively charged surface patch of the Bcl-xL core formed by the cluster of arginine residues including R100, R102, R103 (Fig. 3c; Supplementary Fig. 5g). This cluster of arginine residues may thus provide an electrostatic docking site that stabilizes the various hydrophobic and polar α1–α2 IDR—folded core interactions described above. The side-chains of N52 and N66, which become negatively charged upon deamidation, were also proximal to the arginine residues cluster in the structure of Bcl-xL S62E, suggesting a similar mechanism of stabilization of the α1–α2 IDR—folded core interaction upon N66 deamidation (Supplementary Fig 5h).

The α1–α2 IDR—folded core interaction observed in the solution structure of Bcl-xL S62E exhibited a closed conformation of the BH3 binding groove, which is incompatible with pro-

apoptotic BH3 domain binding partners. In addition to this allosteric regulation of BH3 binding, the α1–α2 IDR–folded core interaction would also directly compete with the binding of p53 to Bcl-xL (Supplementary Fig. 6a), as shown using a fluorescence anisotropy assay (Supplementary Fig. 6b, c). The three arginine residues within α2–α3 of Bcl-xL that bind the modified α1–α2 IDR are also present in Bcl-2 (Fig. 3d), which is also phosphorylated within the α1–α2 IDR[14–16], suggesting a common mechanism of PTM-dependent autoregulation. Other Bcl-2 protein family members, including Mcl-1, Bax and Bak, exhibit similar core structures but considerably shorter α1–α2 IDRs that lack PTM sites[40,41] (Fig. 1a) and the cluster of surface-exposed arginine residues (Fig. 3d).

Similarity between solution and nanodisc-anchored Bcl-xL

Bcl-xL is known to localize to the cytoplasm as well as to mitochondrial and other cellular membranes (summarized in[36]); however, the *in vitro* structural results described above regarding interactions between the α1–α2 IDR and the Bcl-xL folded core were performed in the absence of membranes. To investigate the conformational features of Bcl-xL in the presence of membranes, we analyzed ^{15}N-labeled full length Bcl-xL (including the 22 residue-long C-terminal transmembrane domain) that was anchored to membrane mimetic nanodiscs using NMR spectroscopy. The 2D ^{1}H-^{15}N HSQC spectrum of nanodisc-anchored, full length Bcl-xL (Supplementary Fig. 8a, magenta spectrum) was similar to that of Bcl-xL (lacking the C-terminal transmembrane domain) recorded in aqueous solution for which resonances are assigned (Supplementary Fig. 8a, orange spectrum), although, due to the large aggregate size of nanodisc-anchored full length Bcl-xL and lower protein concentration, the former spectrum exhibited broader resonances and reduced signal intensity. The similarity of these two spectra allowed assignment of a large portion of the dispersed resonances for nanodisc-anchored, full length Bcl-xL (103 of 226 possible non-proline HN resonances; Supplementary Fig. 8a,c,d). The assigned resonances span both the folded core and α1–α2 IDR of nanodisc-anchored Bcl-xL and exhibit small chemical shift perturbations (CSPs; <0.12 ppm) relative to the spectrum of Bcl-xL in solution. In particular, small CSPs were observed for several resonances within the α1–α2 IDR and the region of the folded core that binds the α1–α2 IDR (resonances labeled in red and blue, respectively, in Supplementary Fig. 8a). Notably, the indole resonance of W57 within the α1–α2 IDR, which binds to the folded core (*vide supra*), exhibited essentially identical chemical shift values in the two samples (Supplementary Fig. 8a, inset). These results are consistent with previous results from Yao, *et al.*[36], which showed through the analysis of 2D ^{1}H-^{15}N HSQC spectra that, in the absence of residues 45–84 of the α1–α2 IDR, the folded core of nanodisc-anchored Bcl-xL closely resembled that of solution Bcl-xL lacking the C-terminal transmembrane domain. These results also showed that the C-terminal transmembrane domain was inserted into the lipid bilayer of nanodiscs. Our results show that the presence of the α1–α2 IDR does not alter the mechanism of nanodisc anchoring or the conformation of the folded core of Bcl-xL. Furthermore, our results demonstrate that interactions between the α1–α2 IDR and the folded core of Bcl-xL are preserved in nanodisc-anchored, full length Bcl-xL. While the nanodiscs used here do not mimic the lipid composition and dynamics of the outer mitochondrial membrane, our results do suggest that the autoregulatory interactions between the α1–α2 IDR and the folded core of Bcl-xL discussed

above for solution Bcl-xL may be preserved in mitochondrial Bcl-xL. The cellular results discussed below further support this view (*vide infra*).

The α2–α3 Arg cluster senses IDR modifications

Based upon our structural investigations of Bcl-xL S62E, we hypothesized that electrostatic interactions between a positively charged cluster of arginine residues between α2 and α3 and negatively charged moieties introduced by posttranslational modifications within the α1–α2 IDR mediate allosteric control of the BH3 domain binding and anti-apoptotic activity of Bcl-xL. To test this hypothesis, we introduced a charge reversal mutation, Arg 103 to Glu (R103E), within the cluster of three arginines between α2–α3 in Bcl-xL (Fig. 3d). This arginine residue, amongst the three in the cluster, is solvent exposed and its side-chain is oriented outside the BH3 domain binding groove, enabling mutation to Glu to alter binding to the α1–α2 IDR but not alter the core domain structure. ITC measurements showed that Bcl-xL R103E, containing the wild type α1–α2 IDR, tightly bound to BH3 peptides, although with somewhat lower affinities (higher K_D values) than to wild type Bcl-xL (Fig. 3e, Supplementary Table 1). However, the BH3 binding affinity of this mutant was insensitive to mutation of Ser62 to Glu (S62E) or deamidation of N52 and N66 (Fig. 3f, g). These results support our proposal that PTMs promote interactions with α3 of the Bcl-xL folded core by increasing the negative charge of the α1–α2 IDR, i) directly inhibiting p53 binding and ii) allosterically reducing the affinity of the BH3 binding groove for pro-apoptotic BH3 domains.

To assess the biological relevance of this mechanism, we determined the anti-apoptotic activity of wild type Bcl-xL and autoregulation defective mutants in HeLa cells through expression of Cerulean fluorescent protein (CFP)-fused forms of Bcl-xL. Unlike the constructs utilized for *in vitro* studies, these encoded full length Bcl-xL, including the C-terminal membrane insertion domain. Because our *in vitro* results used Bcl-xL constructs that lacked the C-terminal segment, we used full length Bcl-xL, which could normally partition between cytosolic and mitochondrial membrane localization, to test our mechanistic hypotheses. Cells were transfected with vectors that encoded CFP, CFP-Bcl-xL wild type, CFP-Bcl-xL S62E, CFP-Bcl-xL R103E, and CFP-Bcl-xL S62E, R103E (Fig. 4). The CFP fusion was introduced to enable the selection of cells with comparable expression levels using fluorescence activated cell sorting (FACS). Transfected cells were subjected to several levels of UV irradiation and analyzed by FACS for CFP expression and Annexin V staining, an established early apoptosis marker[42] (Fig. 4a, c; Supplementary Fig. 7). These assays indicated that expression of wild-type Bcl-xL protected against UV-induced apoptosis and that protection was reduced by the S62E phosphomimetic mutation, as previously reported[28,29] (Fig. 4b). The R103E mutant was also less effective than wild-type Bcl-xL in protecting UV-irradiated cells against apoptosis. In the presence of the R103E mutation—predicted to disrupt the α1–α2 IDR-mediated autoinhibitory mechanism—introduction of the S62E mutation did not further reduce protection (Fig. 4c). This observation agreed with *in vitro* ITC binding assays (Fig. 3e–f) and confirmed that a reduction in positive charge at the α2–α3 region of Bcl-xL prevented the stabilization of its inhibitory α1–α2 IDR—folded core interaction driven by negative charges at position 62. Western blot analysis confirmed that all CFP-labeled Bcl-xL constructs were similarly expressed and did not experience

differential degradation (Fig. 4d), validating that the cellular effects of the mutations were due to their effects on the affinity of Bcl-xL for its pro-apoptotic binding partners. Fluorescence cell imaging showed that the CFP-labeled Bcl-xL constructs exhibited comparable localization to intracellular membranes (those of mitochondria and ER), which was not altered upon UV irradiation (Supplementary Fig. 9). This observation indicated that mutation of residues within the IDR, or that interact with the IDR, did not alter the membrane localization of Bcl-xL. However, these mutations did alter Bcl-xL function, suggesting strongly that the α1–α2 IDR-dependent autoregulatory mechanism functions similarly in C-terminally truncated Bcl-xL constructs in *in vitro* assays and in full-length Bcl-xL in cells, a substantial proportion of which is anchored to mitochondrial membranes (Supplementary Fig. 9).

Expression of wild-type or R103E Bcl-xL was associated with low level, UV-induced phosphorylation of S62 (Fig. 4d). However, the observation that Bcl-xL S62E was a poorer inhibitor of apoptosis than the wild-type protein suggested that S62 phosphorylation was incomplete under these UV treatment conditions. Conversely, the S62E mutant, representing stoichiometric phosphorylation of this residue, enabled maximal, α1–α2 IDR-dependent down-regulation of Bcl-xL's anti-apoptotic activity.

Finally, we immunopurified the CFP-Bcl-xL constructs and analyzed the level of coimmunoprecipitation of the pro-apoptotic partners, BIM, BAX [a pro-apoptotic effector which exhibits a BH3 domain that binds to and is inhibited by Bcl-xL[43]], and p53. Both BIM and BAX exhibited substantial coimmunoprecipitation with most of the CFP-Bcl-xL constructs but not with the S62E mutant (Fig. 4d). This observation is in agreement with our ITC and FACS results showing a reduction in BH3 binding or anti-apoptotic activity, respectively, of Bcl-xL S62E *versus* wild-type Bcl-xL and no further effect of the S62E mutant when introduced into the R103E mutant (Fig. 4a–c). These coimmunoprecipitation assays reported on the formation of complexes of Bcl-xL with endogenous, full-length, BH3 domain-containing proteins in cells and agreed with our *in vitro* binding assays performed with synthetic BH3 domain peptides.

Intriguingly, while cells expressing Bcl-xL R103E exhibited higher levels of apoptosis than those expressing wild-type Bcl-xL, both constructs exhibited similar abilities to sequester BIM and BAX (as monitored by coimmunoprecipitation; Fig. 4d). However, the R103E Bcl-xL mutation was previously shown to disrupt binding to p53 *in vitro*[8], and was associated with reduced sequestration of p53 in UV-treated cells (Fig. 4d), while *in vitro* it only modestly reduced Bcl-xL binding to pro-apoptotic BH3 domains (Fig. 1c, Fig. 3e, Supplementary Table 1). These observations suggest that the heightened apoptosis in cells expressing Bcl-xL R103E was due to its reduced ability to sequester p53. Overall, the results of our cellular assays support that the S62E phosphomimetic mutation reduced anti-apoptotic activity by, i) directly reducing sequestration of p53 and ii) allosterically reducing sequestration of pro-apoptotic Bcl-2 family proteins with BH3 domains. PTMs within the α1–α2 IDR promote interactions with the Bcl-xL folded core that directly inhibit p53 binding and simultaneously engage the allosteric pathway that modulates BH3 domain binding affinity.

DISCUSSION

Synergy between IDRs and folded domains enhances the functional versatility of proteins[1]. While folded domains are well adapted to perform catalysis and specific molecular recognition, IDRs, by virtue of their enrichment in modifiable amino acids and plasticity, through often weak and transient interactions, can integrate diverse cellular signals to regulate the function of covalently bonded folded domains. The internal α1–α2 IDR of Bcl-xL has been known to integrate a variety of posttranslational modification signals that modulate its anti-apoptotic activity but heretofore the mechanism of this autoregulation was unknown. We have shown that the unmodified, >50 residue long α1–α2 IDR of Bcl-xL is highly flexible and solvent exposed, making it accessible for signaling inputs by enzymes that perform posttranslational modifications. Upon phosphorylation on S62 or deamidation of N52 and N66, which both increase negative charge, the central region of the α1–α2 IDR binds to a cluster of arginine residues on the surface of the Bcl-xL folded domain, triggering a structural rearrangement within the distal binding groove that reduces affinity for pro-apoptotic BH3 domains. NMR data suggested that autoregulatory interactions between the α1–α2 IDR and folded core are similar for solution and nanodisc-anchored Bcl-xL (Supplementary Fig. 8). Together with data showing that the autoregulatory mechanism is active for Bcl-xL in cells, a significant portion of which is localized to mitochondrial membranes, the NMR data suggest that this mechanism may be active for mitochondrial Bcl-xL. The evolution of internal IDRs within Bcl-xL and Bcl-2 affords responsiveness to diverse apoptotic signals that contribute to their specific functions. By experiencing posttranslational modifications from different modifying enzymes, activated under different stress stimuli, these IDRs may differentially tune the activity of various anti-apoptotic members of the Bcl-2 family of proteins under specific sets of circumstances, such as aberrant mitotic spindle assembly in the case of Bcl-xL[26]. This evolutionary strategy towards specific autoregulation affords functional versatility within certain Bcl-2 family of proteins, all of which exhibit significant conservation of sequence and structure within their folded domains. For example, anti-apoptotic Mcl-1 also contains a N-terminal autoregulatory IDR[44,45]. In contrast, other anti-apoptotic (Bcl-W, A1) and pro-apoptotic effector (BAX, BAK, BOK) Bcl-2 family members lack autoregulatory IDRs (Fig. 1A; Bcl-W, A1 and BOK not shown)[46]. The presence of IDRs within these apoptotic regulators may thus contribute to their role as ‘molecular computers’ capable of integrating a diverse range of pro-death and pro-survival signals to control cell fate. This integration occurs not only through modulation of the relative expression levels of various anti- and pro-apoptotic Bcl-2 family members, but also through the fine tuning of their affinities for various binding partners through posttranslational modifications within autoregulatory IDRs, as illustrated here for Bcl-xL.

The surface of Bcl-xL engaged by the posttranslationally modified α1–α2 IDR is also a binding site for the DNA binding domain (DBD) of p53[8]; this latter interaction sequesters cytosolic p53 and inhibits BAX-dependent apoptosis[9]. The BH3 binding groove, comprised of α4–α5, and the abutted α2–α3 allosteric regulatory site serve as a two-way conduit for signal transmission (Figure 5). In one direction, in response to DNA damage-induced nuclear p53 activation[47], PUMA binding to Bcl-xL causes α3 to unfold and allosterically

triggers p53 release and apoptosis[9,48]. In the opposite direction, posttranslational modification of residues within the α1–α2 IDR in response to various apoptotic signals allosterically contracts the BH3 binding groove, freeing pro-apoptotic Bcl-2 family proteins to trigger apoptosis. In addition, by engaging the arginine cluster between α2 and α3, which otherwise binds to the DBD of p53, the IDR of Bcl-xL may release cytosolic p53 to activate BAX and apoptosis. This second pro-apoptotic mechanism further illustrates how functional versatility can be achieved by autoregulatory IDRs. Our study illustrates functional synergy between a folded domain and a disordered region of an apoptotic regulatory protein, Bcl-xL, and clearly demonstrates the capacity of IDRs within multi-domain proteins to serve as conduits for the transmission of diverse signaling inputs.

ONLINE METHODS

Reagents

Human Bcl-xL, lacking the 22 C-terminal residues (to improve solubility) and IDR-truncated Bcl-xL (Bcl-xL ΔIDR), lacking residues 45–84 of the α1–α2 IDR and the 22 C-terminal residues were cloned into pET28 (EMD Biosciences) and pET21 (Novagen) plasmids respectively. Point mutations were introduced with a QuickChange II-Gold site-directed mutagenesis kit (Quiagen) according to the manufacturer protocol. Primer DNA was synthesized by International DNA Technologies Inc. DNA purification was performed with Zyppy Plasmid Miniprep kit (Zymo Research) or Maxiprep kit (Invitrogen). DNA sequencing was performed by the Hartwell Center for Bioinformatics and Biotechnology. Human BID (sequence QEDIIRNIARHLAQVGDSMDRSIPP or EDIIRNIARHLAQVGDSMDRSI-ethylene diamine-Fluorescein), BIM (sequence DNRPEIWIAQELRRIGDEFNAYYAR) BH3 peptides and BCL-xL IDR peptides (residues 44–72; 44–72 phosphorylated at S62; 44–72 N52D, N66D; 52–66 phosphorylated at S62; 52–66 S62E) were synthesized using standard Fmoc-based chemistry by the Hartwell Center for Bioinformatics and Biotechnology, St. Jude Children's Research Hospital and HPLC purified to >98% purity.

Protein expression and purification

Bcl-xL, Bcl-xL ΔIDR, mutant Bcl-xL and p53 1–360 were expressed and purified as previously described[8,49]. All proteins were expressed in E. coli BL21(DE3) expression strain. Unlabeled proteins were expressed in LB media, isotopically labeled proteins in MOPS minimal media[50] supplemented with the appropriate labeling reagents. Culture media were grown at 37 °C until their optical density at 600 nm (OD_{600}) reached a value of 0.6, then induced with 0.5 mM IPTG for 5 hours at 37 °C or 16 hours at 18 °C and harvested. Bcl-xL-expression cells were lysed by osmotic shock in a buffer containing 25 mM Tris, 500 mM NaCl, 5 mM imidazole, 20% w/v sucrose, 1 mg/mL lysozime, pH 8.0. The soluble fraction of the lysate was then purified by Ni affinity chromatography followed by cleavage of the 6×His tag with restriction grade thrombin (Novagen) and anion exchange chromatography using mono-dispersed Q–sepharose resin. This step allows for a complete resolution of native monomeric, IDR deamidated and dimeric Bcl-xL obtained after the Ni affinity step. The whole purification procedure was performed in Tris buffer with either an imidazole or NaCl gradient and pH 8.0 or 7.0 for the Ni-affinity or anion exchange steps,

respectively. The preparation of the fluorescein labeled Bcl-xL C151S, S2C construct was described previously[8]. His-tagged full-length Bcl-xL was purified from inclusion bodies solubilized in 6 M Guanidine Hydrochloride containing 25 mM Tris at pH 8 by Ni affinity chromatography. Bcl-xL was eluted from the Ni resin with an imidazole gradient under denaturing conditions and then further purified by reverse-phase HPLC over a C4 resin with elution by an acetonitrile gradient in the presence of 0.1% trifluoroacetic acid. The eluent was then flash frozen and the solvent removed by lyophilization. Protein identity was confirmed using mass spectrometry and NMR spectroscopy.

In vitro deamidation of Bcl-xL

Bcl-xL was deamidated at N52, N66 by incubation for 48 hours at 37 °C in buffer containing 25 mM Tris, 150 mM NaCl, pH 8.0 at a protein concentration of 200 μM. The identity of the deamidated protein product was confirmed by native gel electrophoresis and intact mass determination.

Isothermal Titration Calorimetry

All ITC experiments were performed over 19 injections of 2 μL each at 25 °C in 20 mM Tris, 40 mM NaCl, pH 7.0, with a MicroCal ITC200 instrument. Data were analyzed with the MicroCal ITC plugins within the Origin suite (OriginLab). Titrations were performed in duplicate or triplicate.

Binding between Bcl-xL and BID, BIM BH3 peptides—BH3 peptide solutions, at nominal concentrations of 50 or 100 μM were prepared from dilution of 10–20 mM DMSO stocks into the flow-through buffer resulting from buffer exchange of the Bcl-xL cell samples. These BH3 peptide syringe samples were titrated into Bcl-xL, at nominal concentrations of 5 or 10 μM, previously buffer exchanged in a 10 KDa cutoff Centricon device (Millipore). The DMSO concentration in the cell sample was carefully matched to that of the syringe sample. The exact peptide or protein concentration of each sample was verified after dilution or buffer exchange.

Binding between Bcl-xL ΔIDR and Bcl-xL IDR peptides—These titrations were performed as above, using starting peptide concentrations in the syringe of 1 or 2 mM and Bcl-xL ΔIDR concentrations in the cell of 100 or 200 μM. The syringe samples were prepared by directly dissolving the lyophilized peptides into buffer resulting from buffer exchange of the Bcl-xL ΔIDR cell samples. Due to the acidity of lyophilized peptides, the pH was carefully matched to that of the cell component before performing the titrations.

Nuclear Magnetic Resonance

^{15}N-labeled Bcl-xL (wild type or N52, N66 deamidated); ^{15}N-labeled Bcl-xL ΔIDR; ^{15}N-, ^{13}C-labeled Bcl-xL S62E were prepared at the indicated concentrations in 10 mM sodium phosphate, pH 7.0, 40 mM NaCl, 0.01% (w/v) NaN_3 and 8% ^2H_2O. Data were acquired on Bruker 600-MHz and 800-MHz spectrometers equipped with cryogenically cooled, triple-resonance single-axis gradient probes. Spectra were processed using TopSpin (Bruker Biospin) and analyzed with CARA software. Two-dimensional ^{1}H-^{15}N correlation TROSY spectra were acquired at 25 °C on 200 μM samples, using standard Bruker pulse sequences

using 8–16 scans, 2,048 × 256 complex points and spectral windows of 14 ppm × 32 ppm in the ^{1}H and ^{15}N dimensions, respectively. {^{1}H} -^{15}N heteronuclear NOE experiments were collected at 25 °C using 32 scans and 2,048 × 300 complex points using similar spectral windows as above on samples containing 0.5 mM protein concentration (Bcl-xL, Bcl-xL S62E). The recycle delay was 1 s for TROSY experiments and 4 s for heteronuclear NOE experiments. For titrations of Bcl-xL IDR peptides with natural isotopic abundance into isotope labeled Bcl-xL ΔIDR, peptide solutions were prepared in the buffer described above at concentrations ranging between 40 and 60 mM and the pH was adjusted to 7.0. Aliquots of these peptide samples were incrementally added to isotope labeled Bcl-xL ΔIDR samples (200 μM). Peptide concentrations ranged between 100 μM or 1 mM to 4 or 6 mM. A slight dilution (10%) of the protein samples occurred over the course of the titrations due to addition of the peptide solution aliquots. The following three-dimensional experiments were performed on Bcl-xL S62E samples for resonance assignment and structure calculation: HNCACB, CBCA(co)NOH, HNCO, HN(ca)CO for backbone assignment (2.2 mM sample); ^{13}C-edited aliphatic and aromatic HSQC-NOESY and ^{15}N-edited TROSY-NOESY for side-chain assignment and distance restraints (1.8 mM sample). Three-dimensional experiments were collected using 8–16 scans over 2,048 × 48–64 × 80–200 complex points and processed with linear prediction and zero filling in the indirect dimensions with spectral windows of 12–14 ppm (^{1}H), 32 ppm (^{15}N), 18 ppm (^{13}C HNCO, HN(ca)CO), 70 ppm, (^{13}C, HNCACB, CBCA(co)NH), 40 ppm (^{13}C aromatic NOESY; offset 120 ppm), 44 ppm (^{13}C aliphatic NOESY; offset: 24 ppm). A NOE mixing time of 100 ms was used in all cases. An equivalent ^{15}N-edited TROSY-NOESY spectrum was also measured on wild type Bcl-xL at a concentration of 0.6 mM using 32 scans per increment.

Solution structure calculation

Structure calculations of Bcl-xL S62E was performed using the program Cyana[51]. Simulated annealing in torsion angle space was performed over 50,000 steps for each run on 400 structures with the 20 models scoring the lowest target function representing the final NMR structure. Distance restraints were generated from volumes of NOESY cross-peaks (integrated with CARA) using the Cyana CALIBA tool. Dihedral restraints were generated from available assignments using the program TALOS+[52]. Helical hydrogen bond restraints (i to i-4) were applied between residues that showed lack of water exchange peaks in three-dimensional NOESY spectra in combination with α-helical backbone torsion angle restraints. Calculations were performed iteratively with correction of restraints calibration and assignments until no further improvement of the target function could be attained. Structures were minimized using the model_minimize routine in the program CNS[53] using an all-energy terms potential, with 1,000 steps and a relative permeativity value of 80. The quality of the models was assessed with the Protein Structure Validation Suite[54]. Structure determination details and statistics are provided in Supplementary Table 2. The Ramachandran statistics for the 20 lowest energy models were as follows. 98.8% of all residues were in favored regions of the Ramachandran plot, 0.5% were in generously allowed regions and 0.7% were in disallowed regions.

Nanodisc sample of full length Bcl-xL

Protein powder (2.5 mg of lyophilized material) was solubilized in 0.5 mL of phosphate buffer (25 mM sodium phosphate, pH 6.5, 2 mM DTT, 1 mM EDTA) supplemented with 100 mM Decylphoshocholine (DePC) detergent, and 50 uL of D_2O. The solution was centrifuged and the supernatant fraction was used to prepare Bcl-xL in nanodiscs as described previously[36]. A 2D ^{1}H-^{15}N HSQC spectrum was recorded using 256 scans with 1024 × 128 complex points and spectral widths of 15.6 × 32 ppm in the ^{1}H and ^{15}N dimensions, respectively, using a Bruker 800 MHz spectrometer equipped with cryogenically cooled, triple-resonance single-axis gradient probe.

Fluorescence Anisotropy

Fluorescence anisotropy measurements were performed at 25 °C using a Horiba Fluorolog 3 spectrofluorimeter with a 3 mM path-length, 45 μL volume quartz cuvette with excitation wavelength of 494 nM and emission wavelength of 521 nM over 5 seconds acquisition periods. The concentration of fluorescein labeled BID BH3 peptide (FAM-BID BH3) was 10 nM and that of fluorescein labeled Bcl-xL C151S S2C (FITC-Bcl-xL) was 100 nM in all assays. Samples were prepared in 10 mM sodium phosphate, pH 7.0, 40 mM NaCl. The equation used to fit the competition titration between Bcl-xL S62E and FITC-Bcl-xL for binding to p53 1–360 was described previously[9].

Cell culture and fluorescence activated cell sorting (FACS) analysis

HeLa cells (American Type Culture Collection) were plated at 10^5 cells/mL (0.5 mL in 24-well plates) in Dulbecco's modified Eagle's medium supplemented with 10% FCS and with 2 mM glutamine, penicillin and streptomycin, transiently transfected for 24 h with 0.5 μg of the indicated Cerulean or Cerulean–Bcl-xL constructs (cloned in pcDNA3.1 vector, Invitrogen) with Lipofectamine. Transfected cells were then UV irradiated (2.5, 5, 10 mJ/cm^2) and incubated for an additional 16 h. Supernatant medium and trypsinized cells were collected and stained with APC-labeled annexin V (eBiosciences), and cell death was analyzed by FACS. A total of 10^4 cells were analyzed for each sample; each condition was tested using three independent samples. After FACS analysis, remaining samples were pooled, harvested, lysed and analyzed by coimmunoprecipitation as described below.

Immunoprecipitation and western blot analysis

Cells were lysed in 0.4 mL ice-cold buffer containing 50 mM Tris, 150 mM NaCl, 1 mM EDTA and 0.5% NP-40, pH 7.4. Cell lysates were incubated with 20 μL Protein A/G beads (Santa Cruz Biotechnology) supplemented with 1 μg anti-GFP antibody (mixed 7.1 and 13.1 clones; Roche; at 1:2,000 dilution) for 2 h at 4 °C, washed four times with cold lysis buffer and eluted by boiling in 50 μL XT sample buffer (Bio-Rad). The protein concentration of total lysate aliquots was determined based upon their optical density at 280 nm. Normalized amounts of total lysate or immunoprecipitated samples were analyzed by SDS-PAGE and western blot. Total lysates were analyzed for GFP (mixed 7.1 and 13.1 clones; Roche; at 1:2,000 dilution), Bcl-xL (antibody clone H-5; Santa Cruz Biotechnology; at 1:200 dilution), S62-phosphorylated Bcl-xL (antibody sc-101644; Santa Cruz Biotechnology; at 1:200 dilution), BIM (antibody B7929, Sigma-Aldrich at 1:2,000 dilution), BAX (antibody clone

N20; Santa Cruz Biotechnology; at 1:200 dilution), p53 (Antibody clone DO-1, Santa Cruz Biotechnology; at 1:1,00 dilution) and Actin (antibody clone 5C5; Santa Cruz Biotechnology; at 1:1,000 dilution). Immunoprecipitated samples were analyzed for GFP, BIM, BAX and p53 as described above. Validation of antibodies used in these assays can be found on the manufacturers' websites.

Confocal microscopy

HeLa cells were plated on 4-well glass chamber slides and transiently transfected with indicated Cerulean expressing constructs (Cerulean, Cerulean Bcl-xL WT, S62E, R103E, S62E-R103E) and Calreticulin-RFP (OriGene RC100040) using Lipofectamine™ 2000 transfection reagent as per the manufacturers' instructions (Invitrogen). 24 h after transfection cells were either UV irradiated (10 mJ/cm^2) or not and supplemented with fresh medium containing Q-VD-OPh (20 μM; MP Biomedicals), and incubated for an additional 16 h. Cells were then stained with MitoTracker Green (ThermoFisher, M7514) for 20 minutes. Confocal microscopy was performed using a Marianas spinning disk confocal imaging system (Intelligent Imaging Innovations/3i) consisting of a CSU-22 confocal head (Yokogowa Electric Corporation, Japan); solid-state diode-pumped laser launch (3i) with wavelengths of 445 nm, 473 nm, 523 nm, 561 nm, and 658 nm; and a Carl Zeiss Axiovert 200M motorized inverted microscope equipped with a precision motorized XY stage (Carl Zeiss MicroImaging) and spherical aberration correction optics (3i). Images were acquired with a Zeiss Plan-Apochromat 63× 1.4 NA DIC objective and a Cascade II 512 EMCCD camera (Photometrics), using the SlideBook 6 software (3i). For quantitative colocalization analysis, regions around individual cells were drawn and the Pearson's correlation coefficient was assessed by using SlideBook 6 software (3i). Statistical analysis was performed using Graph Pad Prism and Microsoft Office Excel.

DATA AVAILABILITY

Data for the solution structure of Bcl-xL S62E has been deposited to the Protein Data Bank (PDB; accession code: 6BF2) and Biological Magnetic Resonance Bank (BMRB; accession code: 27291). The datasets generated during and/or analzsed during the current study are available from the corresponding author upon request.

Supplementary Material

Refer to Web version on PubMed Central for supplementary material.

Acknowledgments

The authors acknowledge Christy R. Grace (SJCRH) for assistance with NMR experiments and Bob Cassell and Patrick Rodrigues (SJCRH) for peptide synthesis. This work was supported by NIH R01CA082491 and 1R01GM083159 (to R.W.K.); NIH R01GM52735 and R01GM96208 (to D.R.G.); R01 CA179087 and R35 GM118186 (to F.M.M.); National Cancer Institute Cancer Center Support Grants P30CA21765 (to SJCRH) and P30CA030199 (to SBP); and ALSAC (to SJCRH). A.V.F. was the recipient of the Neoma Boadway Fellowship from SJCRH.

References

1. Babu MM, Kriwacki RW, Pappu RV. Structural biology. Versatility from protein disorder. Science. 2012; 337:1460–1461. [PubMed: 22997313]
2. Yeon JH, Heinkel F, Sung M, Na D, Gsponer J. Systems-wide Identification of cis-Regulatory Elements in Proteins. Cell Syst. 2016; 2:89–100. [PubMed: 27135163]
3. Showalter SA, Bruschweiler-Li L, Johnson E, Zhang F, Bruschweiler R. Quantitative lid dynamics of MDM2 reveals differential ligand binding modes of the p53-binding cleft. J Am Chem Soc. 2008; 130:6472–6478. [PubMed: 18435534]
4. Pufall MA, Lee GM, Nelson ML, Kang HS, Velyvis A, Kay LE, McIntosh LP, Graves BJ. Variable control of Ets-1 DNA binding by multiple phosphates in an unstructured region. Science. 2005; 309:142–145. [PubMed: 15994560]
5. Youle RJ, Strasser A. The BCL-2 protein family: opposing activities that mediate cell death. Nat Rev Mol Cell Bio. 2008; 9:47–59. [PubMed: 18097445]
6. Shamas-Din A, Kale J, Leber B, Andrews DW. Mechanisms of action of bcl-2 family proteins. Cold Spring Harb Perspect Biol. 2013; 5
7. Petros AM, Nettesheim DG, Wang Y, Olejniczak ET, Meadows RP, Mack J, Swift K, Matayoshi ED, Zhang H, Thompson CB, Fesik SW. Rationale for Bcl-xL/Bad peptide complex formation from structure, mutagenesis, and biophysical studies. Protein Sci. 2000; 9:2528–2534. [PubMed: 11206074]
8. Follis AV, Llambi F, Ou L, Baran K, Green DR, Kriwacki RW. The DNA-binding domain mediates both nuclear and cytosolic functions of p53. Nat Struct Mol Biol. 2014; 21:535–543. [Available on 2014/12/1]. [PubMed: 24814347]
9. Follis AV, Chipuk JE, Fisher JC, Yun MK, Grace CR, Nourse A, Baran K, Ou L, Min L, White SW, Green DR, Kriwacki RW. PUMA binding induces partial unfolding within BCL-xL to disrupt p53 binding and promote apoptosis. Nat Chem Biol. 2013; 9:163–168. [PubMed: 23340338]
10. Maundrell K, Antonsson B, Magnenat E, Camps M, Muda M, Chabert C, Gillieron C, Boschert U, VialKnecht E, Martinou JC, Arkinstall S. Bcl-2 undergoes phosphorylation by c-Jun N-terminal kinase stress-activated protein kinases in the presence of the constitutively active GTP-binding protein Rac1. Journal of Biological Chemistry. 1997; 272:25238–25242. [PubMed: 9312139]
11. Clem RJ, Cheng EH, Karp CL, Kirsch DG, Ueno K, Takahashi A, Kastan MB, Griffin DE, Earnshaw WC, Veliuona MA, Hardwick JM. Modulation of cell death by Bcl-XL through caspase interaction. Proc Natl Acad Sci U S A. 1998; 95:554–559. [PubMed: 9435230]
12. Fang GF, Chang BS, Kim CN, Perkins C, Thompson CB, Bhalla KN. "Loop" domain is necessary for taxol-induced mobility shift and phosphorylation of Bcl-2 as well as for inhibiting taxol-induced cytosolic Accumulation of cytochrome c and apoptosis. Cancer Research. 1998; 58:3202–3208. [PubMed: 9699642]
13. Fujita N, Nagahashi A, Nagashima K, Rokudai S, Tsuruo T. Acceleration of apoptotic cell death after the cleavage of Bcl-X-L protein by caspase-3-like proteases. Oncogene. 1998; 17:1295–1304. [PubMed: 9771973]
14. Kirsch DG, Doseff A, Chau BN, Lim DS, de Souza-Pinto NC, Hansford R, Kastan MB, Lazebnik YA, Hardwick JM. Caspase-3-dependent cleavage of Bcl-2 promotes release of cytochrome c. J Biol Chem. 1999; 274:21155–21161. [PubMed: 10409669]
15. Srivastava RK, Mi QS, Hardwick JM, Longo DL. Deletion of the loop region of Bcl-2 completely blocks paclitaxel-induced apoptosis. Proc Natl Acad Sci U S A. 1999; 96:3775–3780. [PubMed: 10097113]
16. Yamamoto K, Ichijo H, Korsmeyer SJ. BCL-2 is phosphorylated and inactivated by an ASK1/Jun N-terminal protein kinase pathway normally activated at G(2)/M. Mol Cell Biol. 1999; 19:8469–8478. [PubMed: 10567572]
17. Kharbanda S, Saxena S, Yoshida K, Pandey P, Kaneki M, Wang QH, Cheng KD, Chen YN, Campbell A, Sudha T, Yuan ZM, Narula J, Weichselbaum R, Nalin C, Kufe D. Translocation of SAPK/JNK to mitochondria and interaction with Bcl-x(L) in response to DNA damage (vol 275, pg 322, 2000). J Biol Chem. 2000; 275:19433–19433.

18. Basu A, Haldar S. Identification of a novel Bcl-xL phosphorylation site regulating the sensitivity of taxol- or 2-methoxyestradiol-induced apoptosis. Febs Lett. 2003; 538:41–47. [PubMed: 12633850]
19. Du LH, Lyle CS, Chambers TC. Characterization of vinblastine-induced Bcl-xL and Bcl-2 phosphorylation: evidence for a novel protein kinase and a coordinated phosphorylation/dephosphorylation cycle associated with apoptosis induction. Oncogene. 2005; 24:107–117. [PubMed: 15531923]
20. Schmitt E, Beauchemin M, Bertrand R. Nuclear colocalization and interaction between bcl-xL and cdk1(cdc2) duringG(2)/M cell-cycle checkpoint. Oncogene. 2007; 26:5851–5865. [PubMed: 17369848]
21. Zhao R, Oxley D, Smith TS, Follows GA, Green AR, Alexander DR. DNA damage-induced Bcl-x(L) deamidation is mediated by NHE-1 antiport regulated intracellular pH. Plos Biol. 2007; 5:39–53.
22. Asakura T, Maeda K, Omi H, Matsudaira H, Ohkawa K. The association of deamidation of Bcl-xL and translocation of Bax to the mitochondria through activation of JNK in the induction of apoptosis by treatment with GSH-conjugated DXR. International Journal of Oncology. 2008; 33:389–395. [PubMed: 18636161]
23. Upreti M, Galitovskaya EN, Chu R, Tackett AJ, Terrano DT, Granell S, Chambers TC. Identification of the Major Phosphorylation Site in Bcl-xL Induced by Microtubule Inhibitors and Analysis of Its Functional Significance. J Biol Chem. 2008; 283:35517–35525. [PubMed: 18974096]
24. Wei YJ, Sinha S, Levine B. Dual role of JNK1-mediated phosphorylation of Bcl-2 in autophagy and apoptosis regulation. Autophagy. 2008; 4:949–951. [PubMed: 18769111]
25. Tamura Y, Simizu S, Muroi M, Takagi S, Kawatani M, Watanabe N, Osada H. Polo-like kinase 1 phosphorylates and regulates Bcl-x(L) during pironetin-induced apoptosis. Oncogene. 2009; 28:107–116. [PubMed: 18820703]
26. Terrano DT, Upreti M, Chambers TC. Cyclin-Dependent Kinase 1-Mediated Bcl-x(L)/Bcl-2 Phosphorylation Acts as a Functional Link Coupling Mitotic Arrest and Apoptosis. Mol Cell Biol. 2010; 30:640–656. [PubMed: 19917720]
27. Dho SH, Deverman BE, Lapid C, Manson SR, Gan L, Riehm JJ, Aurora R, Kwon KS, Weintraub SJ. Control of Cellular Bcl-x(L) Levels by Deamidation-Regulated Degradation. Plos Biol. 2013; 11
28. Bah N, Maillet L, Ryan J, Dubreil S, Gautier F, Letai A, Juin P, Barille-Nion S. Bcl-xL controls a switch between cell death modes during mitotic arrest (vol 5, e1291, 2014). Cell Death Dis. 2014; 5
29. Kim SY, Song XX, Zhang L, Bartlett DL, Lee YJ. Role of Bcl-xL/Beclin-1 in interplay between apoptosis and autophagy in oxaliplatin and bortezomib-induced cell death. Biochem Pharmacol. 2014; 88:178–188. [PubMed: 24486574]
30. Terrano DT, Upreti M, Chambers TC. Cyclin-dependent kinase 1-mediated Bcl-xL/Bcl-2 phosphorylation acts as a functional link coupling mitotic arrest and apoptosis. Mol Cell Biol. 2010; 30:640–656. [PubMed: 19917720]
31. Maiuri MC, Le Toumelin G, Criollo A, Rain JC, Gautier F, Juin P, Tasdemir E, Pierron G, Troulinaki K, Tavernarakis N, Hickman JA, Geneste O, Kroemer G. Functional and physical interaction between Bcl-X-L and a BH3-like domain in Beclin-1. Embo J. 2007; 26:2527–2539. [PubMed: 17446862]
32. Tyler-Cross R, Schirch V. Effects of amino acid sequence, buffers, and ionic strength on the rate and mechanism of deamidation of asparagine residues in small peptides. J Biol Chem. 1991; 266:22549–22556. [PubMed: 1939272]
33. Muchmore SW, Sattler M, Liang H, Meadows RP, Harlan JE, Yoon HS, Nettesheim D, Chang BS, Thompson CB, Wong SL, Ng SL, Fesik SW. X-ray and NMR structure of human Bcl-xL, an inhibitor of programmed cell death. Nature. 1996; 381:335–341. [PubMed: 8692274]
34. Sattler M, Liang H, Nettesheim D, Meadows RP, Harlan JE, Eberstadt M, Yoon HS, Shuker SB, Chang BS, Minn AJ, Thompson CB, Fesik SW. Structure of Bcl-xL-Bak peptide complex: recognition between regulators of apoptosis. Science. 1997; 275:983–986. [PubMed: 9020082]

35. Lee EF, Czabotar PE, Smith BJ, Deshayes K, Zobel K, Colman PM, Fairlie WD. Crystal structure of ABT-737 complexed with Bcl-xL: implications for selectivity of antagonists of the Bcl-2 family. Cell death and differentiation. 2007; 14:1711–1713. [PubMed: 17572662]
36. Yao Y, Fujimoto LM, Hirshman N, Bobkov AA, Antignani A, Youle RJ, Marassi FM. Conformation of BCL-XL upon Membrane Integration. J Mol Biol. 2015; 427:2262–2270. [PubMed: 25731750]
37. Yao Y, Bobkov AA, Plesniak LA, Marassi FM. Mapping the interaction of pro-apoptotic tBID with pro-survival BCL-XL. Biochemistry. 2009; 48:8704–8711. 2762941. [PubMed: 19670908]
38. Wysoczanski P, Mart RJ, Loveridge EJ, Williams C, Whittaker SB, Crump MP, Allemann RK. NMR solution structure of a photoswitchable apoptosis activating Bak peptide bound to Bcl-xL. J Am Chem Soc. 2012; 134:7644–7647. [PubMed: 22515821]
39. Hagn F, Klein C, Demmer O, Marchenko N, Vaseva A, Moll UM, Kessler H. BclxL changes conformation upon binding to wild-type but not mutant p53 DNA binding domain. J Biol Chem. 2010; 285:3439–3450. 2823462. [PubMed: 19955567]
40. Basu A, DuBois G, Haldar S. Posttranslational modifications of Bcl2 family members - a potential therapeutic target for human malignancy. Front Biosci. 2006; 11:1508–1521. [PubMed: 16368533]
41. Kutuk O, Letai A. Regulation of Bcl-2 family proteins by posttranslational modifications. Curr Mol Med. 2008; 8:102–118. [PubMed: 18336291]
42. Vermes I, Haanen C, Steffensnakken H, Reutelingsperger C. A Novel Assay for Apoptosis - Flow Cytometric Detection of Phosphatidylserine Expression on Early Apoptotic Cells Using Fluorescein-Labeled Annexin-V. J Immunol Methods. 1995; 184:39–51. [PubMed: 7622868]
43. Czabotar PE, Lee EF, Thompson GV, Wardak AZ, Fairlie WD, Colman PM. Mutation to Bax beyond the BH3 Domain Disrupts Interactions with Pro-survival Proteins and Promotes Apoptosis. J Biol Chem. 2011; 286:7123–7131. [PubMed: 21199865]
44. Domina AM, Vrana JA, Gregory MA, Hann SR, Craig RW. MCL1 is phosphorylated in the PEST region and stabilized upon ERK activation in viable cells, and at additional sites with cytotoxic okadaic acid or taxol. Oncogene. 2004; 23:5301–5315. [PubMed: 15241487]
45. Maurer U, Charvet C, Wagman AS, Dejardin E, Green DR. Glycogen synthase kinase-3 regulates mitochondrial outer membrane permeabilization and apoptosis by destabilization of MCL-1. Mol Cell. 2006; 21:749–760. [PubMed: 16543145]
46. Youle RJ, Strasser A. The BCL-2 protein family: opposing activities that mediate cell death. Nature reviews. Molecular cell biology. 2008; 9:47–59. [PubMed: 18097445]
47. Chipuk JE, Bouchier-Hayes L, Kuwana T, Newmeyer DD, Green DR. PUMA couples the nuclear and cytoplasmic proapoptotic function of p53. Science. 2005; 309:1732–1735. [PubMed: 16151013]
48. Follis AV, Llambi F, Merritt P, Chipuk JE, Green DR, Kriwacki RW. Pin1-Induced Proline Isomerization in Cytosolic p53 Mediates BAX Activation and Apoptosis. Mol Cell. 2015; 59:677–684. [PubMed: 26236013]
49. Chipuk JE, Fisher JC, Dillon CP, Kriwacki RW, Kuwana T, Green DR. Mechanism of apoptosis induction by inhibition of the anti-apoptotic BCL-2 proteins. Proc Natl Acad Sci U S A. 2008; 105:20327–20332. [PubMed: 19074266]
50. Neidhardt FC, Bloch PL, Smith DF. Culture Medium for Enterobacteria. J Bacteriol. 1974; 119:736–747. [PubMed: 4604283]
51. Guntert P. Automated NMR structure calculation with CYANA. Methods Mol Biol. 2004; 278:353–378. [PubMed: 15318003]
52. Shen Y, Delaglio F, Cornilescu G, Bax A. TALOS plus : a hybrid method for predicting protein backbone torsion angles from NMR chemical shifts. Journal of Biomolecular Nmr. 2009; 44:213–223. [PubMed: 19548092]
53. Brunger AT, Adams PD, Clore GM, DeLano WL, Gros P, Grosse-Kunstleve RW, Jiang JS, Kuszewski J, Nilges M, Pannu NS, Read RJ, Rice LM, Simonson T, Warren GL. Crystallography & NMR system: A new software suite for macromolecular structure determination. Acta crystallographica. Section D, Biological crystallography. 1998; 54:905–921. [PubMed: 9757107]
54. Bhattacharya A, Tejero R, Montelione GT. Evaluating protein structures determined by structural genomics consortia. Proteins-Structure Function and Bioinformatics. 2007; 66:778–795.

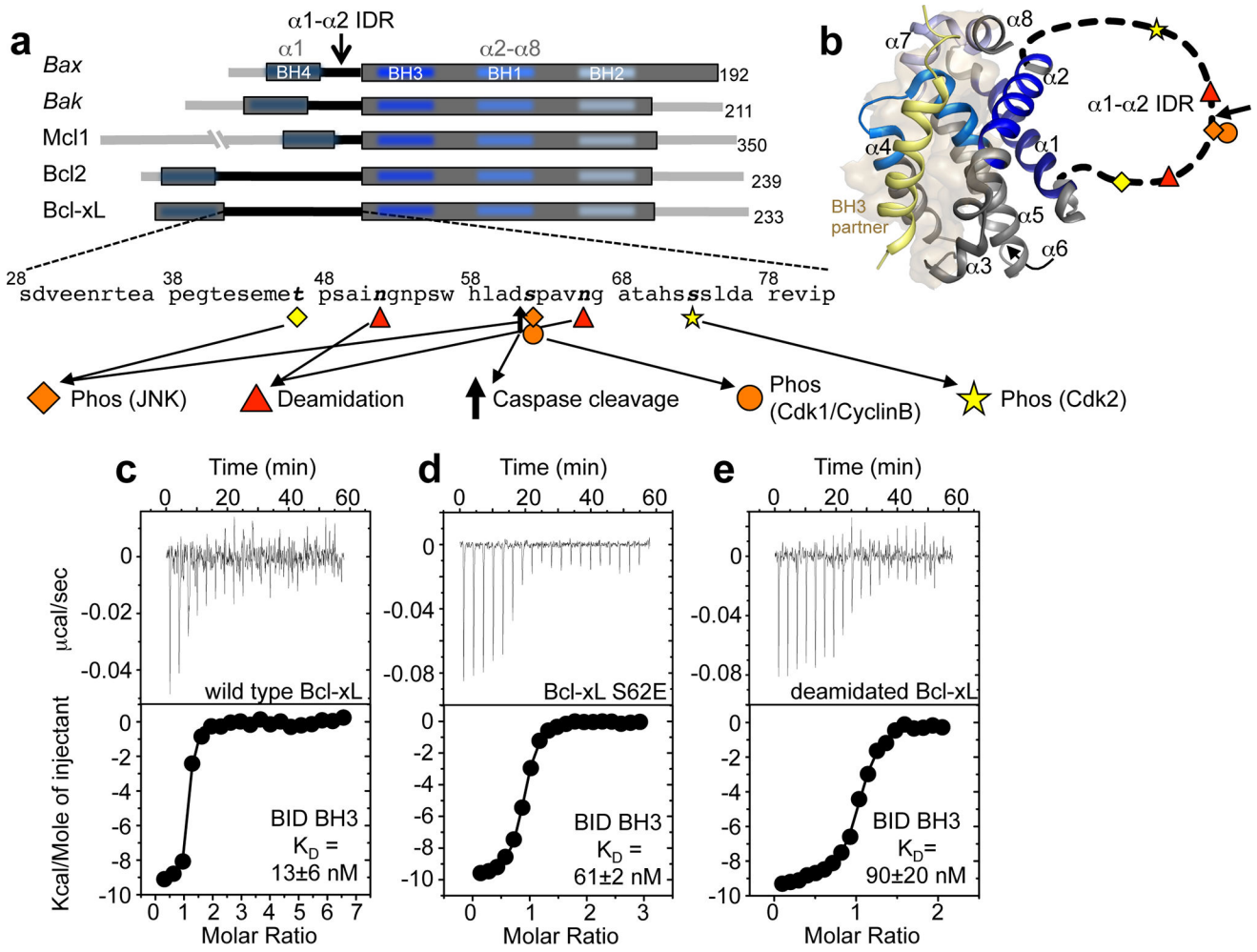

Figure 1.

PTMs within the α1–α2 IDR of Bcl-xL down regulate its anti-apoptotic function. **a**. Schematic alignment of multi-domain Bcl-2 proteins (pro-apoptotic effectors, Bax and Bak; anti-apoptotic, Mcl1, Bcl-2, and Bcl-xL). The sequence if the α1–α2 IDR of Bcl-xL is shown at the bottom, with known PTM sites indicated. **b.** Structure of Bcl-xL (pdb: 1g5j), showing the four BH domains in different shades of blue, the BH3 domain partner and corresponding binding groove on the surface of Bcl-xL in yellow; the α1–α2 IDR is indicated as a dashed line. **c–e.** Isothermal titration calorimetry thermographs and curve fits for titrations of a BID BH3 domain peptide into wild-type Bcl-xL (**c**), a α1–α2 IDR phosphomimetic Bcl-xL S62E mutant (**d**), and α1–α2 IDR deamidated Bcl-xL (**e**). K_D values are the average and s.e.m. of two or three independent titrations.

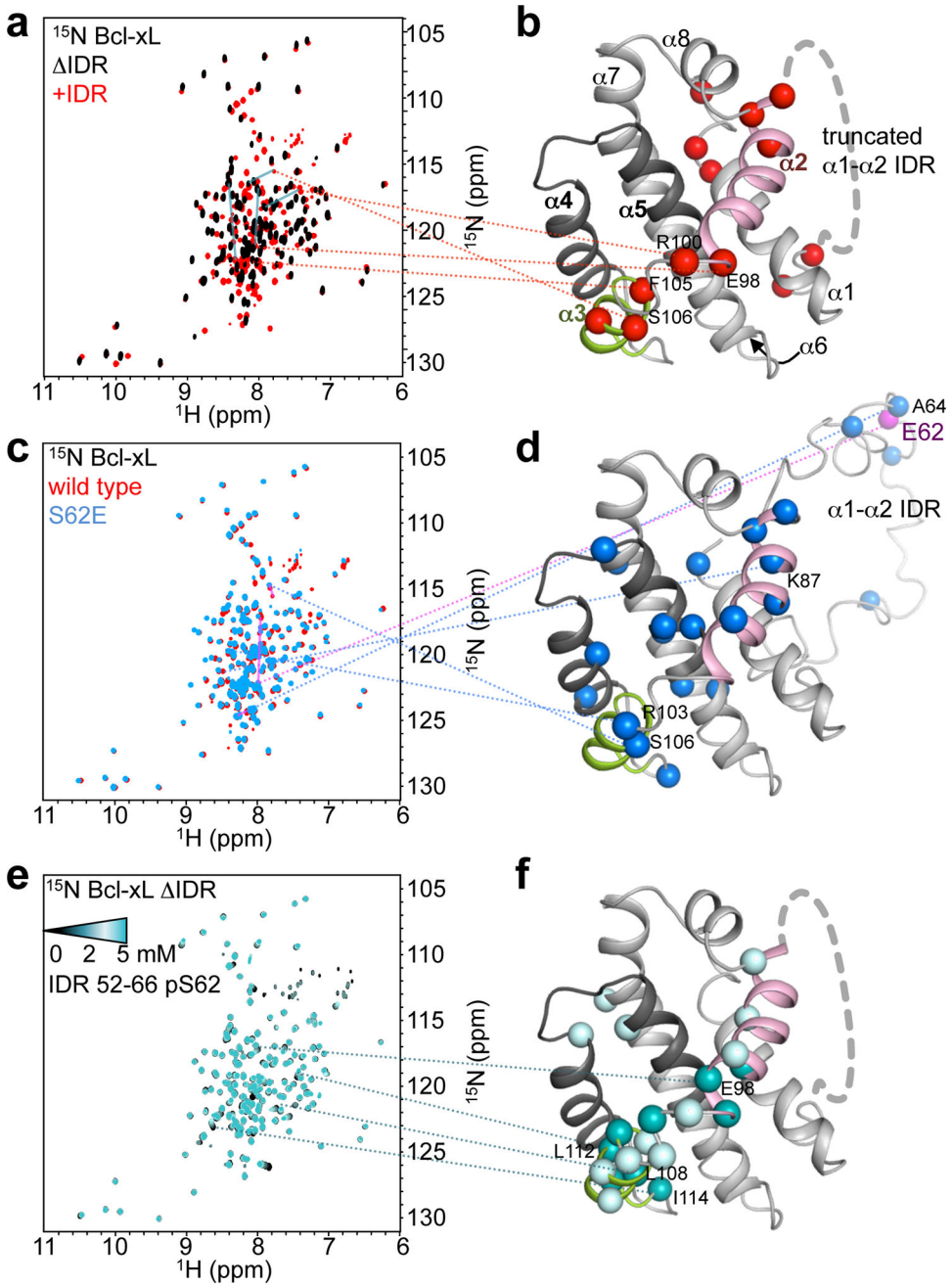

Figure 2.

NMR evidence of an interaction between the α1–α2 IDR and folded core of Bcl-xL. **a.** Overlaid ^{1}H-^{15}N TROSY spectra of Bcl-xL with truncated α1–α2 IDR (Bcl-xL ΔIDR, black) or full length α1–α2 IDR (red). **b.** Structure mapping of residues within the folded core of Bcl-xL whose resonances exhibit significant (>1 σ) chemical shift perturbations (CSPs) between the two spectra, marked with red spheres. Dashed lines provide visual links between some of these residues and the corresponding resonances in panel **a**. Solid lines connect equivalent resonances in the two overlaid spectra. **c–d.** Analogous representations comparing wild-type Bcl-xL, containing the full length α1–α2 IDR (red), with the

phosphomimetic Bcl-xL S62E mutant (light blue). Residues exhibiting significant CSPs are marked with light blue spheres in panel **d**. **e–f.** Titration of a synthetic peptide spanning residues 52–66 of Bcl-xL, phosphorylated at S62, into ^{15}N-Bcl-xL ΔIDR (black to cyan gradient). Residues exhibiting significant CSPs are marked with light (>1 σ) or dark (>2 σ) cyan spheres in panel **f**.

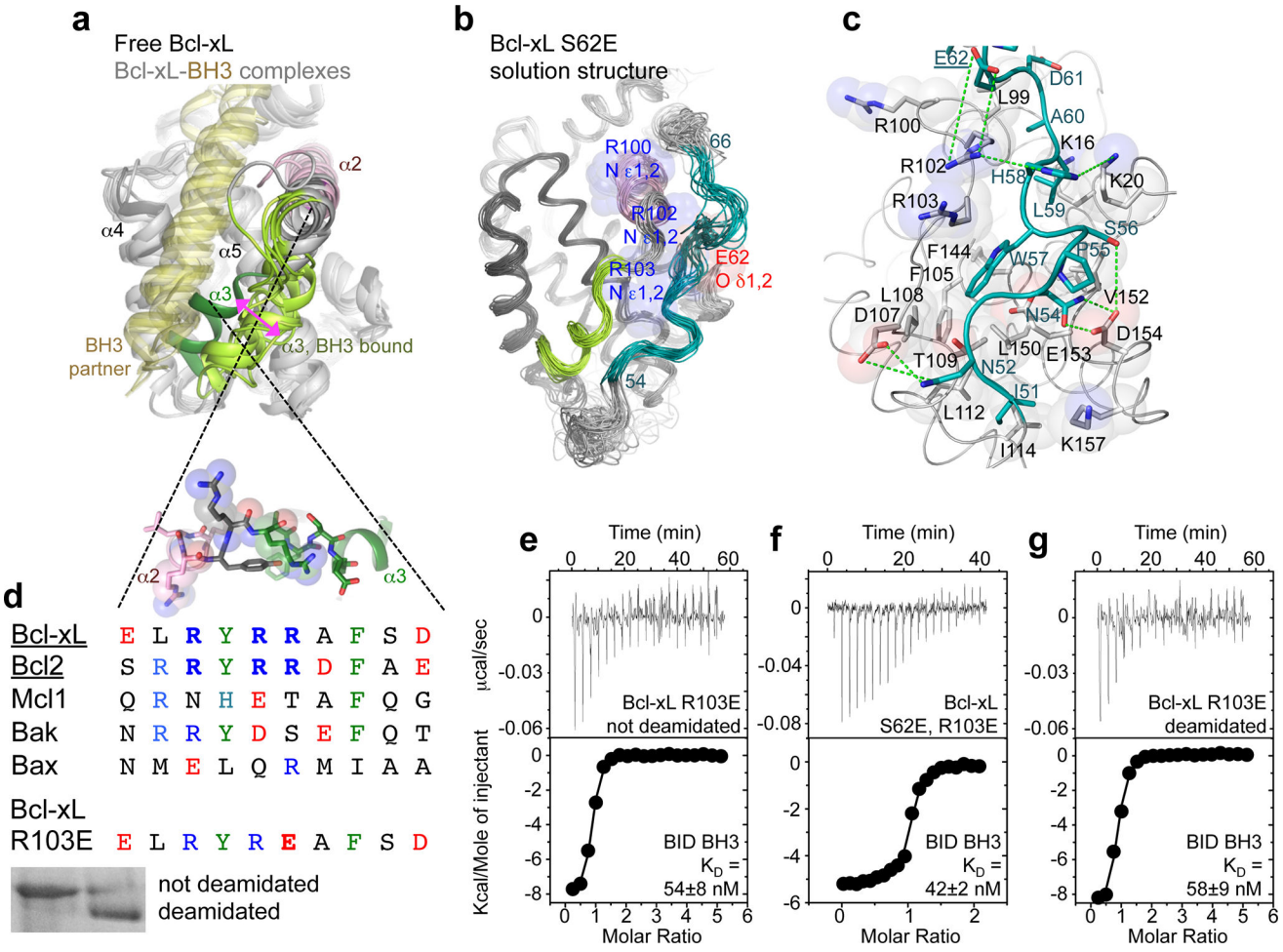

Figure 3.

Inhibition of the BH3-binding associated repositioning of Bcl-xL α2–α3 relative to α4–α5 by the α1–α2 IDR. **a.** Structure alignment between unbound Bcl-xL (pdb 1r2d, dark grey) and Bcl-xL (light grey) – BH3 domain (green) complexes (complexes with BAK, pdb 1g5j; BAX, pdb 3pl7; BAD, pdb 1bxl; PUMA, pdb 2m04; BIM, pdb 4qvf; BID, pdb 4qve; and Beclin1, pdb 2pon). The pink arrow marks the repositioning of α3 upon binding of BH3 domains. **b.** Solution structure of Bcl-xL S62E highlighting the central portion of the α1–α2 IDR (residues 54–66, dark cyan) interacting with the folded protein core near arginine residues at the α2–α3 junction. **c.** Close up view of the α1–α2 IDR (dark cyan) – folded core (grey) interaction with labeled side chains (IDR residues, dark cyan; core residues, black). Green dashes indicate possible electrostatic or hydrogen bonding interactions. **d.** Structure (top) and alignment (center) of the α2–α3 junction sequences in various multi-domain Bcl-2 proteins and the Bcl-xL R103E mutant. The bottom panel shows the native-PAGE mobility-shift of Bcl-xL R103E upon deamidation of N52 and N66 (full gel is provided in Supplementary Fig. 10). **e–g.** ITC thermographs and curve fits for titrations of a BID BH3 domain peptide into Bcl-xL R103E (**e**), Bcl-xL S62E R103E (**f**), and deamidated Bcl-xL R103E (**g**). K_D values are the average and s.e.m. of two or three independent titrations.

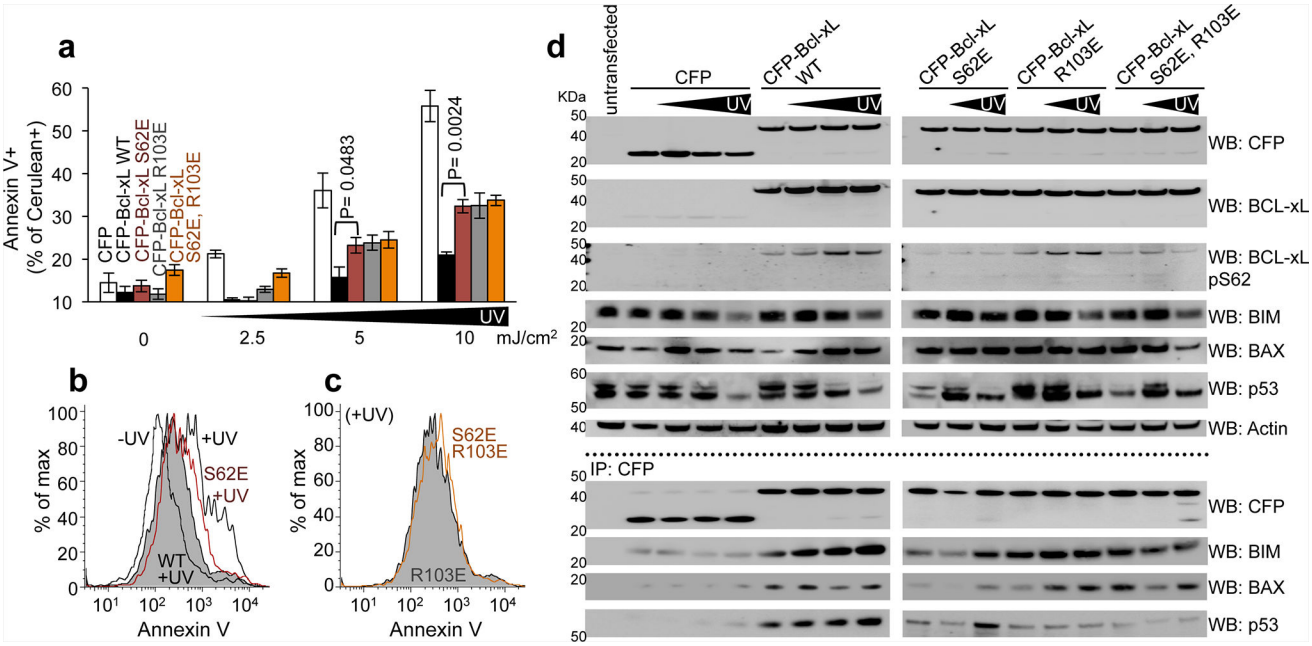

Figure 4.

Modulation of the anti-apoptotic activity of Bcl-xL by mutations in the α1–α2 IDR and α2–α3. **a.** Fluorescence-activated cell sorting (FACS) analysis of HeLa cells transfected with Cerulean fluorescent protein (CFP) - Bcl-xL fusion constructs in the absence and presence of increasing UV irradiation. Cerulean only (CFP), white; Bcl-xL wild-type (WT), black; Bcl-xL S62E, maroon; Bxl-xL R103E, grey; Bcl-xL S62E - R103E, orange (N = 3 experimental replicates; error bars, s.e.m.; p values, 95% confidence intervals). **b–c.** FACS populations for (**b**) CFP-transfected HeLa cells in the absence of UV (left trace; '-UV'), 16 hours after 10 mJ/cm^2 UV irradiation (right trace; '+UV'), UV-irradiated cells transfected with CFP-Bcl-xL wild-type (solid grey; 'WT + UV'), or CFP-Bcl-xL S62E (maroon trace; 'S62E + UV') and (**c**) UV irradiated cells transfected with CFP-Bcl-xL R103E (solid grey; 'R103E') or CFP-Bcl-xL S62E - R103E (orange trace; 'S62E R103E'). **d.** Western blotting analysis of total cell lysates (top seven blots) for Cerulean, Bcl-xL, S62 phosphorylated Bcl-xL, BIM. BAX. p53 and Actin. The bottom four blots show analyses for Cerulean. BIM. BAX and p53 after immunoprecipitation of Cerulean (full gels are provided in Supplementary Fig. 10).

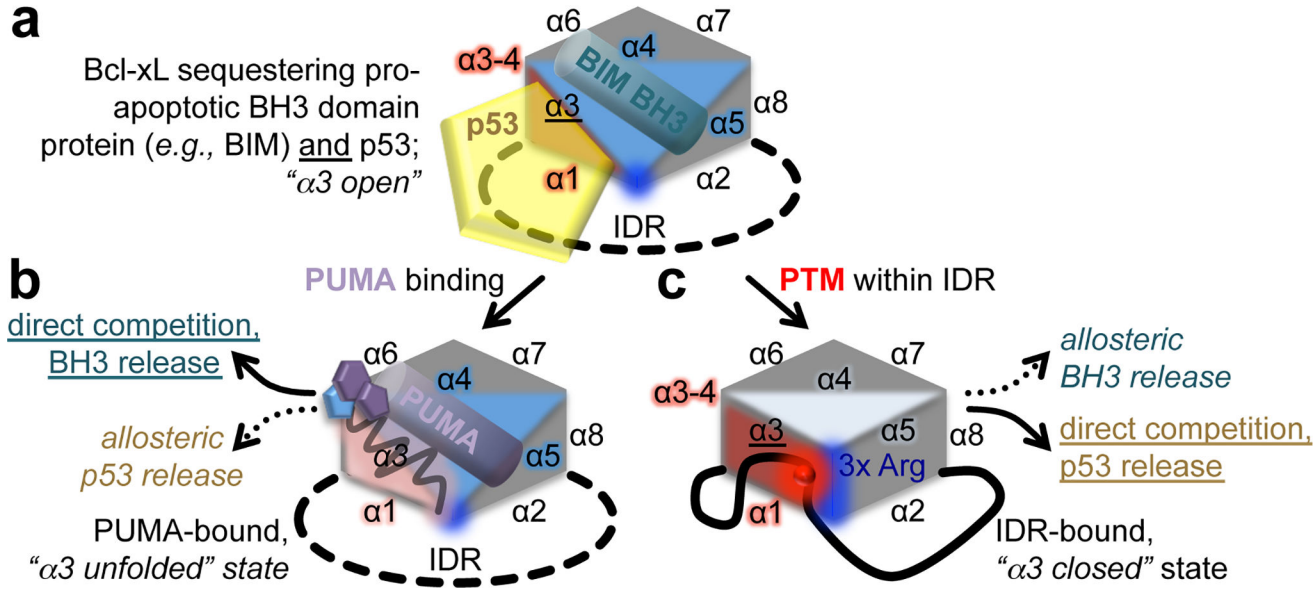

Figure 5.

Schematic illustration of the proposed dual mechanism of allosteric regulation of Bcl-xL enabled by PTMs in the α1–α2 IDR and structural plasticity of α3. **a.** Bcl-xL inhibits apoptosis by sequestering both pro-apoptotic BH3 domain-containing proteins (e.g., BIM) and p53. The binding sites on Bcl-xL for BH3 domains and p53 are adjacent but non-overlapping, and are allosterically coupled. This is termed the *"α3 accessible"* state. **b.** The binding of PUMA to Bcl-xL directly displaces BH3 domain-containing proteins (e.g., BIM) and allosterically releases p53 from the distal site, enabling the released proteins to induce apoptosis. This is termed the PUMA-bound, *"α3 unfolded"* state. **c.** In a reversal of the allosteric pathway illustrated in **b**, PTMs within the α1–α2 IDR promote its interactions with the α2-α region of the folded core, displacing p53, and also allosterically remodeling the BH3 binding groove, releasing BH3 domain-containing proteins from Bcl-xL. As in **b**, the released proteins induce apoptosis. This is termed the IDR-bound, *"α3 inaccessible"* state.